Blazed high-efficiency x-ray diffraction via transmission through arrays of nanometer-scale mirrors

Ralf K. Heilmann,[1,*] **Minseung Ahn,**[1] **Eric M. Gullikson,**[2] **and Mark L. Schattenburg**[1]

[1]*Space Nanotechnology Laboratory, MIT Kavli Institute for Astrophysics and Space Research, Massachusetts Institute of Technology, Cambridge, MA 02026, USA*
[2]*Center for X-Ray Optics (CXRO), Lawrence Berkeley National Laboratory, Berkeley, CA 94720, USA*
[*]*Corresponding author: ralf@space.mit.edu*

Abstract: Diffraction gratings are ubiquitous wavelength dispersive elements for photons as well as for subatomic particles, atoms, and large molecules. They serve as enabling devices for spectroscopy, microscopy, and interferometry in numerous applications across the physical sciences. Transmission gratings are required in applications that demand high alignment and figure error tolerances, low weight and size, or a straight-through zero-order beam. However, photons or particles are often strongly absorbed upon transmission, e.g., in the increasingly important extreme ultraviolet (EUV) and soft x-ray band, leading to low diffraction efficiency. We demonstrate the performance of a critical-angle transmission (CAT) grating in the EUV and soft x-ray band that for the first time combines the advantages of transmission gratings with the superior broadband efficiency of blazed reflection gratings via reflection from nanofabricated periodic arrays of atomically smooth nanometer-thin silicon mirrors at angles below the critical angle for total external reflection. The efficiency of the CAT grating design is not limited to photons, but also opens the door to new, sensitive, and compact experiments and applications in atom and neutron optics, as well as for the efficient diffraction of electrons, ions, or molecules.

OCIS codes: (050.1950) Diffraction gratings; (050.7330) Volume gratings; (230.1360) Beam splitters; (230.1950) Diffraction gratings; (230.4000) Microstructure fabrication; (230.4040) Mirrors; (260.6048) Soft x-rays; (260.7200) Ultraviolet, extreme; (300.6320) Spectroscopy, high-resolution; (300.6560) Spectroscopy, x-ray; (340.7480) X-rays, soft x-rays, extreme ultraviolet (EUV); (350.1260) Astronomical optics; (350.4990) Particles; (020.1335) Atom optics

References and links

1. D. T. Attwood, *Soft X-Rays and Extreme Ultraviolet Radiation: Principles and Applications* (Cambridge University Press, 1999).
2. D. W. Keith, M. L. Schattenburg, H. I. Smith, and D. E. Pritchard, "Diffraction of atoms by a transmission grating," Phys. Rev. Lett. **61**, 1580-1583 (1988).
3. M. Arndt, *et al.*, "Wave-particle duality of C-60 molecules," Nature **401**, 680-682 (1999).
4. P. R. Berman, *Atom Interferometry* (Academic Press, 1997).
5. C. R. Canizares, *et al.*, "The Chandra high-energy transmission grating: Design, fabrication, ground calibration, and 5 years in flight," PASP **117**, 1144-1171 (2005).

#94888 - $15.00 USD Received 14 Apr 2008; revised 15 May 2008; accepted 22 May 2008; published 28 May 2008

6. M. L. Schattenburg, "From nanometers to gigaparsecs: The role of nanostructures in unraveling the mysteries of the cosmos," J. Vac. Sci. Technol. B **19**, 2319-2328 (2001).
7. T. Wilhein *et al.*, "A slit grating spectrograph for quantitative soft x-ray spectroscopy," Rev. Sci. Instrum. **70**, 1694-1699 (1999).
8. B. Blagojevic *et al.*, "Imaging transmission grating spectrometer for magnetic fusion experiments," Rev. Sci. Instrum. **74**, 1988-1992 (2003).
9. D. Stutman *et al.*, "Spectroscopic imaging diagnostics for burning plasma experiments," Rev. Sci. Instrum. **76**, 023505 (2005).
10. J. Kirz, C. Jacobsen, M. Howells, "Soft x-ray microscopes and their biological applications," Q. Rev. Biophys. **28**, 33-130 (1995).
11. G. Schmahl *et al.*, "Phase-contrast studies of biological specimens with the x-ray microscope at BESSY," Rev. Sci. Instrum. **66**, 1282-1286 (1995).
12. A. G. Klein and S. A. Werner, "Neutron Optics," Rep. Prog. Phys. **46**, 259-335 (1983).
13. A. I. Ioffe, V. S. Zabiyakin, and G. M. Drabkin, "Test of a diffraction grating neutron interferometer," Phys. Lett. A **111**, 373-375 (1985).
14. H. H. Solak, "Nanolithography with coherent extreme ultraviolet light," J. Phys. D Appl. Phys. **39**, R171-R188 (2006).
15. P. P. Naulleau, C. H. Cho, E. M. Gullikson, and J. Bokor, "Transmission phase gratings for EUV interferometry," J. Synch. Rad. **7**, 405-410 (2000).
16. A. G. Michette and C. J. Buckley, *X-ray Science and Technology* (Institute of Physics Publishing, 1993).
17. A. E. Franke *et al.*, "Super-smooth x-ray reflection grating fabrication," J. Vac. Sci. Technol. B **15**, 2940-2945 (1997).
18. A. Rasmussen *et al.*, "Grating arrays for high-throughput soft x-ray spectrometers," Proc. SPIE **5168** 248-259 (2004).
19. J. F. Seely *et al.*, "Efficiency of a grazing-incidence off-plane grating in the soft-x-ray region," Appl. Opt. **45**, 1680-1687 (2006).
20. K. Flanagan *et al.*, "Spectrometer concept and design for x-ray astronomy using a blazed transmission grating," Proc. SPIE **6688**, 66880Y (2007).
21. M. Born and E. Wolf, *Principles of Optics* (Cambridge University Press, 1998).
22. M. G. Moharam, D. A. Pommet, E. B. Grann, T. K. Gaylord, "Stable implementation of the rigorous coupled-wave analysis for surface-relief gratings - enhanced transmittance matrix approach," J. Opt. Soc. Am. A **12**, 1077-1086 (1995).
23. M. Ahn, R. K. Heilmann, and M. L. Schattenburg, "Fabrication of ultrahigh aspect ratio freestanding gratings on silicon-on-insulator wafers," J. Vac. Sci. Technol. B **25**, 2593-2597 (2007).
24. R. K. Heilmann, C. G. Chen, P. T. Konkola, M. L. Schattenburg, "Dimensional metrology for nanometer-scale science and engineering: Towards sub-nanometer accurate encoders," Nanotechnology **15**, S504-S511 (2004).
25. B. L. Henke, E. M. Gullikson, and J. C. Davis, "X-ray interactions - photoabsorption, scattering, transmission, and reflection at E=50-30,000 eV, Z=1-92," Atomic Data and Nuclear Data Tables **54**, 181-342 (1993).
26. D. Hambach, G. Schneider, and E. M. Gullikson, "Efficient high-order diffraction of extreme-ultraviolet light and soft x-rays by nanostructured volume gratings," Opt. Lett. **26**, 1200-1202 (2001).
27. H. L. Marshall, "A soft x-ray polarimeter designed for broadband x-ray telescopes," Proc. SPIE **6688**, 66880Z (2007).
28. A. Momose, "Recent advances in x-ray phase imaging," Jpn. J. Appl. Phys. **44**, 6355-6367 (2005).
29. M. Engelhardt *et al.*, "High-resolution differential phase contrast imaging using a magnifying projection geometry with a microfocus x-ray source," Appl. Phys. Lett. **90**, 224101 (2007).
30. C. David, B. Nöhammer, H. H. Solak, and E. Ziegler, "Differential x-ray phase contrast imaging using a shearing interferometer," Appl. Phys. Lett. **81**, 3287-3289 (2002).
31. H. C. Kang *et al.*, "Nanometer linear focusing of hard x rays by a multilayer Laue lens," Phys. Rev. Lett. **96**, 127401 (2006).
32. A. N. Kurokhtin, A. V. Popov, "Simulation of high-resolution x-ray zone plates," J. Opt. Soc. Am. A **19**, 315-324 (2002).
33. H. Takenaka, S. Ichimaru, and E. M. Gullikson, "EUV beam splitter for use in the wavelength region around 6 nm," J. Electron Spectrosc. Relat. Phenom. **144**, 1043-1045 (2005).
34. J. W. Elam, D. Routkevitch, P. P. Mardilovich, and S. M. George, "Conformal coating on ultrahigh-aspect-ratio nanopores of anodic alumina by atomic layer deposition," Chem. Mat. **15**, 3507-3517 (2003).
35. A. Anderson *et al.*, "Reflection of thermal Cs atoms grazing a polished glass surface," Phys. Rev. A **34**, 3513-3516 (1986).
36. H. Oberst, Y. Tashiro, K. Shimizu, F. Shimizu, "Quantum reflection of He^* on silicon," Phys. Rev. A **71**, 052901 (2005).
37. A. D. Cronin and B. McMorran, "Electron interferometry with nanogratings," Phys. Rev. A **74**, 061602 (2006).
38. B. Barwick *et al.*, "A measurement of electron-wall interactions using transmission diffraction from nanofabricated gratings," J. Appl. Phys. **100**, 074322 (2006).

#94888 - $15.00 USD Received 14 Apr 2008; revised 15 May 2008; accepted 22 May 2008; published 28 May 2008

39. A. Kalinin, O. Kornilov, W. Schöllkopf, J. P. Toennies, "Observation of mixed fermionic-bosonic helium clusters by transmission grating diffraction," Phys. Rev. Lett. **95**, 113402 (2005).
40. J. D. Perreault and A. D. Cronin, "Using atomic diffraction of Na from material gratings to measure atom-surface interactions," Phys. Rev. A **71**, 053612 (2005).
41. S. Wethekam and H. Winter, "Excitation of fullerene ions during grazing scattering from a metal surface," Phys. Rev. A **76**, 032901 (2007).

1. Introduction

The soft x-ray to EUV region of the electromagnetic spectrum, extending roughly from 0.5 to 50 nm in wavelength, contains many resonances for low to intermediate atomic number elements, and also the so-called water window, rendering it a rich region for elemental identification and for the high-resolution imaging of carbon-containing objects [1]. However, the resulting short ($\sim$ nm to micron) absorption lengths have long prevented the implementation of efficient transmitting diffractive elements that enable microscopes, spectrographs, and interferometers, and maximize the limited photon yield from laboratory sources at these wavelengths. In some applications blazed reflection gratings - which utilize diffracted orders on the same side of the grating as the incident photons - have previously offered higher efficiency, but often at the cost of more demanding alignment and figure requirements, larger weight and size, difficult-to-fabricate grating profiles, or the necessity for complicated multilayer coatings. Compared to photons, absorption lengths for atoms and molecules are even shorter, and devices with nanometer-sized open gaps are required for transmission [2, 3]. Experiments in atom interferometry [4] are often limited by low flux, and efficient diffractive elements could drastically improve contrast and signal-to-noise ratios and thus sensitivity, independent of strong laser-accessible transitions. Progress in this area could lead to advances in many fields, ranging from astronomy [5, 6], plasma [7, 8, 9] and atom [4] physics to the life and environmental sciences [10, 11], as well as in the areas of synchrotron and neutron [12, 13] optics and EUV lithography [14, 15].

Traditional phase-shifting transmission grating design requires the fabrication of regions of periodically alternating complex indices of refraction, n_1 and n_2 (see Fig. 1(a)). For simplicity we assume $n_1 = 1$ (vacuum). The region with index n_2 defines a grating bar. The bars often are supported by a (potentially absorbing) membrane or substrate. Parts of a wave front incident normal to the grating undergo a phase shift $2\pi(d/\lambda)Re(1-n_2)$ upon transmission through the grating bars relative to the parts of the wave front transmitted through the gaps, with d being the grating depth and λ being the wavelength of the incident light. Destructive interference results in the forward direction when the phase shift equals $\pm\pi$. At the same time, diffraction in the first orders is maximized, with theoretical efficiencies as high as $4/\pi^2 \approx 40\%$ in each first order [16]. The angles β_m of the diffracted orders relative to the grating normal are given by the grating equation

$$\frac{m\lambda}{p} = \sin\alpha - \sin\beta_m, \tag{1}$$

where α is the angle of incidence relative to the grating normal, m is the order of diffraction ($m = 0, \pm1, \pm2, ...$), and p is the grating period. For EUV or soft x-ray photons $n_2 = 1-\delta+i\beta$, with $\delta \approx 10^{-3}$-10^{-5}. The resulting large π-phase-shifting grating depths are given by $d_\pi = \lambda/(2\delta)$, often exceeding the absorption lengths by orders of magnitude and turning the phase shifting grating into an inefficient amplitude grating.

EUV and soft x-ray transmission gratings are mainly used in first order, often at efficiencies well below 10%. A suitable grating material can sometimes be found with minimal absorption at a given wavelength that results in total throughput on the order of 40% (e.g., molybdenum at 13.4 nm [15]), but spectrographs often require high efficiency over a broad wavelength band. At

#94888 - $15.00 USD Received 14 Apr 2008; revised 15 May 2008; accepted 22 May 2008; published 28 May 2008

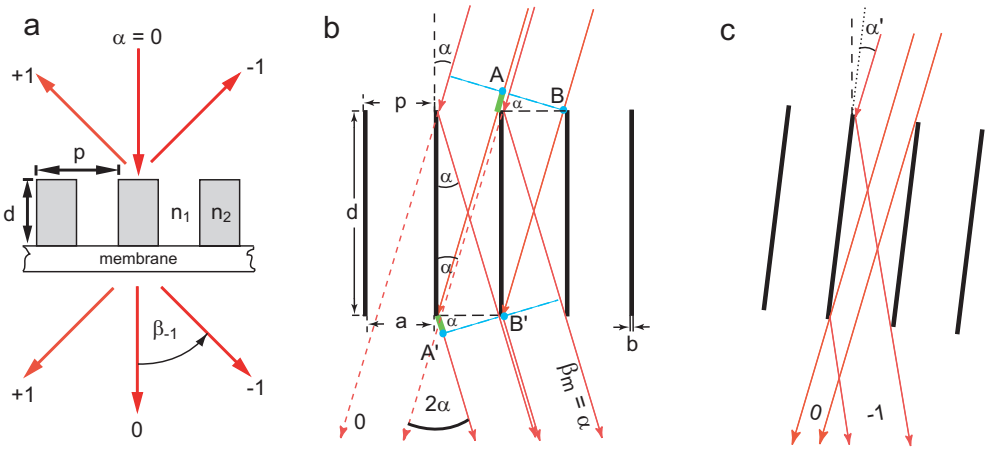

Fig. 1. Comparison of traditional gratings and CAT grating. (a) Schematic of a traditional phase-shifting transmission grating. Reflection gratings utilize diffraction orders on the same side of the grating as the incident beam, and transmission gratings utilize orders on the opposite side of the grating. (b) CAT grating schematic. The path length difference acquired between paths AA' and BB' (in green) determines the condition for the directions where diffraction peaks occur. The special case $\beta_m = \alpha$ is shown. (All photons that exit the grating on the bottom are considered as transmitted, even if they underwent reflection on the grating bar sidewalls.) (c) Schematic of the variable-ratio beam splitter concept. Here rotation of the CAT grating changes the intensity ratio between 0th and -1st order.

shorter wavelengths - where absorption in the grating bars and in the supporting membrane are still tolerable - the gold phase-shifting transmission gratings of the High Energy Transmission Grating Spectrometer (HETGS) on board NASA's Chandra X-ray Observatory were designed for maximum efficiency around $\lambda \approx 0.6$ nm and also achieved close to 40% peak efficiency (sum of $\pm$1st orders) [5].

Blazed reflection gratings for the EUV and x-ray band can mostly avoid efficiency loss from absorption since most photons remain in vacuum, impinging on the grating facets at grazing angles below the critical angle for total external reflection, $\theta_c(\lambda) = (2\delta)^{1/2} \approx 0.5\text{-}10^o$. At the same time blazing can concentrate the diffracted intensity into a small number of desired orders. In the 1.5 to 5 nm wavelength band gold-coated reflection gratings with first order diffraction efficiencies of 10-27% and 10-40% have been demonstrated in in-plane and extreme off-plane mounting geometries, respectively [17, 18, 19]. In the latter case the diffraction behavior becomes highly polarization dependent, which may or may not be desirable, depending on the application.

However, transmission gratings have a number of advantages compared to reflection gratings that make them the preferred choice in numerous important applications. Compared to EUV and x-ray reflection gratings that operate at small angles of grazing incidence - necessitating gratings that are often many cm long along the direction of photon propagation - transmission gratings only need to be a few μm thick. This can result in large mass savings in weight-sensitive applications, such as space based instruments [20]. In imaging applications transmission gratings preserve an undeviated zeroth order beam. Furthermore, transmission gratings are inherently less sensitive to alignment and figure errors than reflection gratings. This is due to the fact that all reflected diffraction orders have experienced a wave vector transfer that depends linearly on small variations γ in the angle of incidence, while the angles of transmitted orders are more weakly dependent on γ.

#94888 - $15.00 USD Received 14 Apr 2008; revised 15 May 2008; accepted 22 May 2008; published 28 May 2008

For example, let us consider the case $p = 100$ nm, $\lambda = 1$ nm and the geometry of Fig. 1(a). A laboratory frame is defined by the incident beam. In the reference frame of the grating the angles of the diffraction orders are given by Eq. (1) above. If we rotate the grating by a small angle γ around the normal to the plane of incidence α changes, and we obtain new angles of diffraction. In the laboratory frame (relative to the incident beam) this results in a rotation of all reflected orders by an angle close to 2γ, while the transmitted orders only rotate by $(\gamma/2)(m\lambda/p)^2$ to first order in γ. In our example this shows that transmitted orders are 3-4 orders of magnitude less sensitive to grating misalignment - or equivalently, grating figure errors - than reflected orders. Such relaxed tolerances can have a significant impact on the cost, weight, and feasibility of instrument designs and resulting instrument performance [20].

Thus, for many applications an "ideal" diffraction grating would combine the advantages of transmission gratings with the high broadband efficiency of a blazed reflection grating.

The critical-angle transmission (CAT) grating design shown in Fig. 1(b) fulfills these requirements. The grating consists of free-standing and nm-thin high aspect-ratio grating bars with smooth sidewalls. Photons are incident at small angles relative to the sidewalls. Most photons only propagate through vacuum and avoid transmission through absorbing media. Blazing is achieved - in analogy to blazed reflection gratings - via efficient reflection off of the grating bar sidewalls acting as mirrors. Transmitted diffraction orders appear at angles β_m where adjacent wave fronts have acquired path length differences equal to integer multiples of the wavelength λ. This general condition for constructive interference is identical to Eq. (1). Clearly, the directions of the transmitted diffraction orders are governed by the grating equation and display significantly lower sensitivity to grating alignment and figure errors than reflected orders. High mirror reflectivity occurs in the direction of specular reflection ($\beta_m = \alpha$), and thus a strong blazing effect is expected at an angle 2α relative to the incident wave. In order to achieve high specular reflectivity in the EUV to x-ray region, we need $\alpha < \theta_c$, and the mirror microroughness should be below 1 nm to minimize scattering losses. Simple geometrical optics suggest that each photon incident upon the gap of width a between mirrors should undergo a single reflection, resulting in $d = a/\tan\alpha$, ranging from about $5a$ to $100a$. The mirror thickness b needs to be much smaller than a to minimize absorption. Aspect ratios for the grating bars should therefore fulfill the challenging requirement $d/b > 100$.

Rotation of the CAT grating around the normal to the plane of incidence by an angle γ changes the direction of the blaze condition by 2γ with minimal displacement of the transmitted ($m \neq 0$) orders. For monochromatic photons changing the direction of the blaze condition continuously "shifts" the diffraction intensity between orders. For example, the CAT grating could be used as a variable-ratio beam splitter in an interferometer, and grating rotation would allow for easy contrast optimization between two neighboring transmitted orders, and thus help to maximize the interferometer signal-to-noise ratio (see also Fig. 1(c)). If the diffraction intensity is concentrated into a single order, a CAT grating could even serve as a compact alignment-insensitive "mirror".

Critical-angle phenomena for neutrons can be described in analogous fashion to the case of x rays. Due to the often cm-wide beams at neutron sources, mirrors based on grazing-incidence reflection can be many meters long and require demanding figure precision. A CAT grating could prove itself useful as a compact and efficient alignment and figure insensitive beam splitter or mirror for cold neutrons.

Since most incident photons only traverse vacuum, the CAT grating design also lends itself to application as a transmission grating for massive particles, such as neutral and charged atoms and molecules, and electrons. The question at hand in these cases is whether the grating bar sidewalls can act as efficient mirrors.

#94888 - $15.00 USD Received 14 Apr 2008; revised 15 May 2008; accepted 22 May 2008; published 28 May 2008

2. CAT grating model

At first sight the CAT grating might look like a confusing hybrid between a transmission and reflection grating. However, it is a true transmission grating, and reflection off of its constituent mirrors only serves as a means for blazing. Following the discussion in Born & Wolf [21] we present a simple theoretical CAT grating model that describes its key physics.

Let us consider a flat plane with a structure that is periodic with period p in one dimension. In the Fraunhofer limit of scalar Kirchhoff diffraction theory the function that describes the diffraction intensity of any 1-D grating consists of two factors. One factor is the grating interference function which only depends on the period of the grating, the wavelength of the incident light, the relative orientation between the incident beam and the direction of periodicity, and the number of grating elements k.

$$I_{grat}(\lambda, p, \alpha, \beta, k) = \left| \frac{\sin kg}{k \sin g} \right|^2, \tag{2}$$

where $g = p(\pi/\lambda)(\sin\beta - \sin\alpha)$. For increasing k, I_{grat} quickly approaches a sum of delta functions with peak positions given by the grating equation. The second factor is the slit intensity function. It describes how an individual grating element or slit interacts with the incident wave. From simple geometric considerations, a function that describes the effects of diffraction due to the finite slit size a and mirror reflection within the slits is given by

$$I_{slit}(\lambda, \alpha, \beta, a, \varepsilon) = \left| \frac{\sin f}{f} \right|^2, \tag{3}$$

where $f = a(\pi/\lambda)(-\sin(\beta+\varepsilon) - \sin(\alpha+\varepsilon))$, and ε is the angle of the mirror surface relative to the grating normal.

We further assume that all photons entering the gap between grating bars are reflected according to the specular reflectivity R of the mirrors, and that all photons hitting the tops of the bars of width b are absorbed. The total diffraction intensity is therefore given by

$$I(\lambda, p, \alpha, \beta, k, a, \varepsilon, R) = I_{grat} I_{slit} R(\alpha + \varepsilon, n_2(\lambda))(a/p), \tag{4}$$

with $n_2(\lambda)$ being the index of refraction of the grating material. This simple model correctly describes the location of the diffraction peaks and the peak location and width of the modulating slit intensity function, and it gives a reasonable estimate for the diffraction efficiency. Of course the efficiency estimate becomes less meaningful in geometries where photons undergo zero or more than one specular reflection ($\alpha \neq \tan^{-1} a/d$).

However, this model completely neglects the three-dimensional character of a CAT grating structure and related effects, such as diffraction within the long grating slots, as well as partial transmission through the grating bars, especially at shorter wavelengths. We therefore also modeled the diffraction efficiency using the rigorous coupled-wave analysis (RCWA) technique, which provides exact solutions of Maxwell's equations for the diffraction of electromagnetic waves from three-dimensional periodic grating structures [22].

3. Results

The challenges in fabricating a CAT grating are the creation of freestanding, nm-thin high aspect-ratio grating bars with sidewalls of sub-nm microroughness. Nanoscale structures that simultaneously exhibit such extreme properties have not been previously fabricated. Our fabrication process is centered around the highly anisotropic etching of silicon crystals in potassium hydroxide (KOH) solution [23]. As a grating substrate we used a <110> SOI wafer with a

#94888 - $15.00 USD Received 14 Apr 2008; revised 15 May 2008; accepted 22 May 2008; published 28 May 2008

10 μm silicon device layer on top of a 2 μm silicon oxide layer. The device layer contains the CAT grating bars that are carefully aligned to the $\{111\}$ planes of the $<110>$ surface, and integrated supporting structures that consist of a coarse support mesh and a 10 mm $\times$ 12 mm release frame (see Fig. 2(a)). A matching release frame was patterned on the back side of the wafer. The oxide layer serves as an etch stop during separate wet etching steps on both sides of the wafer. The device layer was etched anisotropically in KOH solution. This crucial step takes advantage of the high KOH etch rate in the $<110>$ direction, which is more than two orders of magnitude larger than in the $<111>$ directions, and results in high-aspect-ratio grating bars with an almost rectangular cross section, and mirror surfaces primarily consisting of atomically smooth $\{111\}$ silicon crystal lattice planes [23]. The top of our support mesh strips is about 30 μm wide. Due to the presence of additional $\{111\}$ planes that are not normal to the $<110>$ surface the KOH etch produces support mesh sidewalls at a 30^o angle relative to the wafer surface, broadening the support mesh strips by ~ 17 μm on each side (see Fig. 2(a)). Additional process steps designed to eliminate the broadening effect are under development. After removal of the oxide layer and the etch masks the sample is dried in a supercritical dryer to minimize stiction between neighboring grating bars.

The CAT grating prototype investigated in this work has a period of 574 nm, which at the time of fabrication was determined by unrelated factors. The grating module consists of a 0.5 mm-thick window-like frame with four 4×4 mm^2 panes (see Fig. 2(a)). Each pane consists of a 10 μm thick silicon membrane. The membrane is structured into a 10 μm thick support mesh with a period of 70 μm in the plane of the membrane that is defined by contact lithography. The support mesh beams widen from 30 μm at the top to 65 μm at the bottom, leaving a 5 μm wide open gap at the bottom. The open area fraction is therefore close to 7%. The CAT grating bars - patterned by scanning beam interference lithography [24] - are suspended between the support mesh beams [23].

Inspection by scanning electron microscopy (SEM) reveals long and narrow grating bars that are 41 ± 2 nm wide at the top where the KOH etch started, and about 101 ± 1 nm wide at the bottom (see Figs. 2(b) and 2(c)). Approximating the sidewalls as straight lines we obtain a slightly trapezoidal cross section (see Fig. 2(d) and also Fig. 6(d) in Ref. [23]) with an average mirror angle magnitude of 0.17^o relative to the grating normal, an average grating bar aspect ratio $< d/b > \approx 10/0.071 \approx 141$, and an average duty cycle $< b/p >$ of only 0.124. This geometry corresponds to an optimum angle of incidence $\alpha \approx 2.89^o$. This angle is below $\theta_c(\lambda)$ for $\lambda > 2$ nm in the case of Si. Atomic force microscope measurements on a grating bar sidewall of a cleaved sample give a roughness of 0.2 nm (rms) over a 65×65 nm^2 area. Thus we were able to meet or exceed all prototype design goals.

We measured the diffraction efficiency of the above grating sample in transmission at Beam Line 6.3.2 of the Advanced Light Source (ALS) at Lawrence Berkeley National Laboratory. The grating was mounted at the center of a goniometer with its normal along the direction of the incident beam (see Fig. 3). The beam was focused on the detector and had a diameter of ~ 1.1 mm at the sample. The transmitted intensity was measured at a distance of 230 mm from the center of the goniometer by scanning a slit-covered photo diode detector in the vertical plane of dispersion. At normal incidence we obtained the expected symmetrical diffraction pattern shown in Fig. 4(a).

The grating normal was then rotated by $\alpha = 2.8^o$ from the incident photon beam about an axis parallel to the grating bars. Fig. 4(b) shows an example of the observed blazing: The -2nd order peak increases in intensity by a factor > 20. The results also demonstrate the insensitivity of the transmitted diffraction angles to grating rotation: Despite rotation by a rather large angle of 2.8^o, the -2nd order peak moves closer to the 0th transmitted order by only $0.005^o \pm 0.001^o$ in agreement with the value of 0.006^o predicted by Eq. (1).

#94888 - $15.00 USD Received 14 Apr 2008; revised 15 May 2008; accepted 22 May 2008; published 28 May 2008

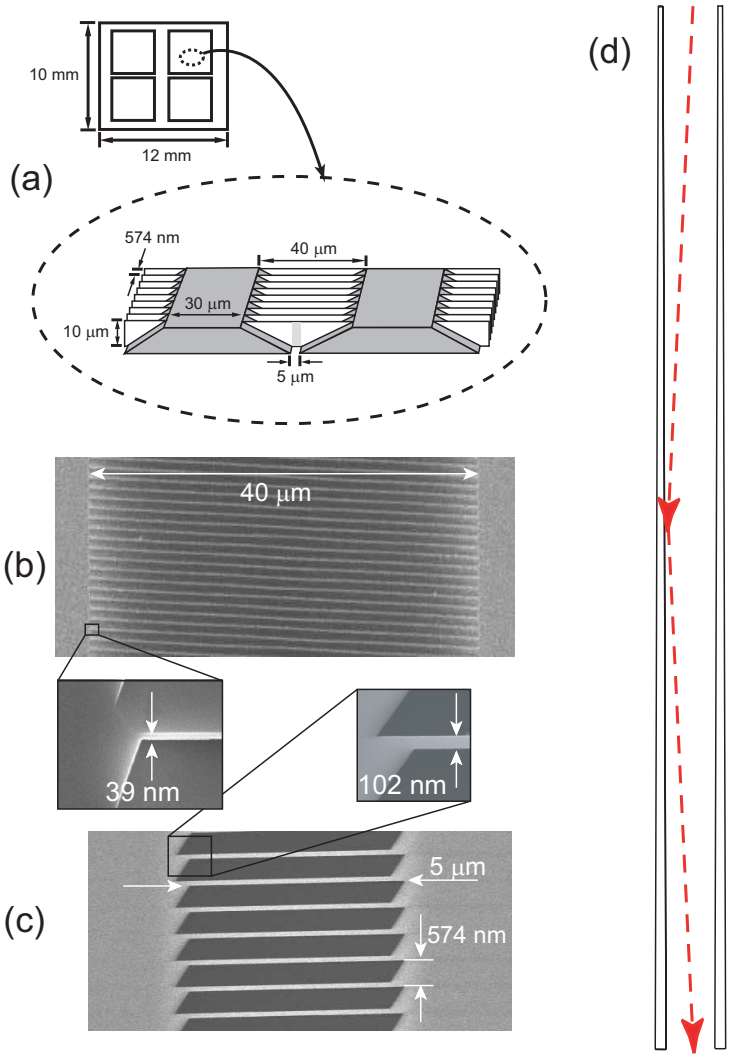

Fig. 2. Structure of the CAT grating sample. (a) Schematic of the grating frame (top) and of the monolithic Si CAT grating structure with the integrated support mesh (dark grey) and the CAT grating bars (white). Only the area above the 5μm open gap (light grey) contributes significantly to transmission. The open area fraction is $\approx 5\mu\text{m}/(40+30)\mu\text{m}$ $\approx$ 7%. (b)-(c) Scanning electron micrographs of the tested CAT grating sample. (b) Top view of the 10μm thick silicon membrane, showing the 40μm long grating bars. Only the central 5μm are open all the way through the membrane. The blow-up shows the narrow grating bar width. (c) Bottom view of the same structure, showing the open gaps. (The blow-ups are not necessarily from the indicated spots.) (d) Schematic cross section of two adjacent grating bars, drawn to scale. The dashed arrows indicate the path of a photon reflecting off a sidewall.

#94888 - $15.00 USD Received 14 Apr 2008; revised 15 May 2008; accepted 22 May 2008; published 28 May 2008

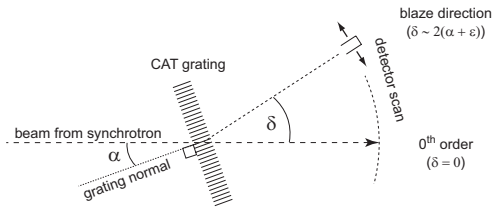

Fig. 3. Schematic of the diffraction efficiency measurements (see text for details).

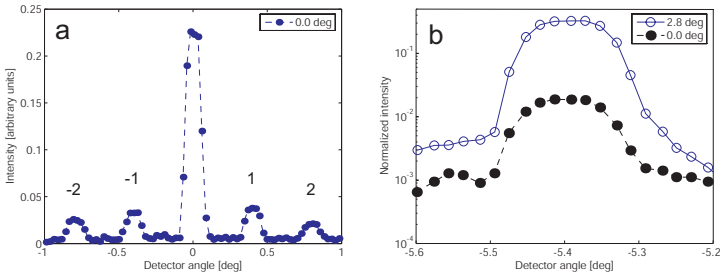

Fig. 4. Detector angle scan data. (a) Transmitted diffraction peaks at $\alpha = 0^o$ and $\lambda = 4.0$ nm (unnormalized). (b) Logarithmic plot of the normalized intensity for the -2nd order transmitted peak at $\alpha = 0^o$ (filled circles) and at $\alpha = 2.8^o$ (open circles) at $\lambda = 27$ nm. Blazing increases the peak intensity more than twenty-fold at this wavelength.

We performed detector scans at wavelengths ranging from 1.62 to 49 nm. At each wavelength we also measured the direct beam for normalization with the sample removed. Fig. 5 shows the results of detector scans at four wavelengths, normalized to the direct beam, the simultaneously measured synchrotron ring current, and the open area fraction of 7%. In the normalization we also took into account the wavelength-dependent partial transmission through the thinnest parts of the support mesh. The dashed line shows the slit transfer function from Eq. (3) times a/p times the reflectivity of Si at an angle $\alpha + \varepsilon = 2.97^o$. It provides an envelope that describes the modulation in the intensity of the diffracted orders due to blazing. The solid line shows the predicted diffraction intensity from Eq. (4). The sharp peaks were convoluted with a Gaussian of the same width as the peak obtained from detector scans through the direct beam to mimic the experimental angular resolution. The data qualitatively follow the simple model: The CAT grating blazes in the direction of specular reflection from the mirror-like sidewalls with a slit intensity function similar to Eq. (3).

The normalized intensities for measured peaks are shown in Fig. 6 at a number of wavelengths, encompassing diffraction orders -1 through -23. The dark diamonds show the sum of the diffraction intensities from those measured peaks that are within the blaze envelope. Solid lines show the predictions from RCWA calculations for the same quantities. For the RCWA calculations we approximate a trapezoidal silicon grating bar profile with sidewalls that are

#94888 - $15.00 USD Received 14 Apr 2008; revised 15 May 2008; accepted 22 May 2008; published 28 May 2008

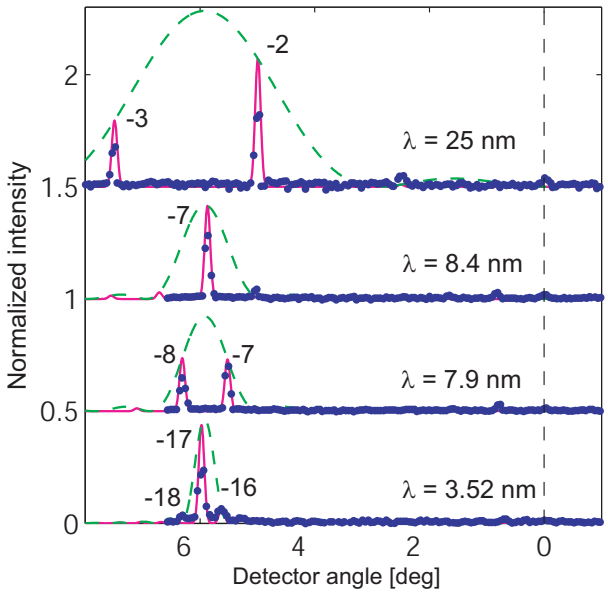

Fig. 5. Comparison of normalized detector angle scan data and the simple model from Eqns. (2)-(4). The results for different wavelengths are shifted for clarity. The peaks under the blaze envelope are labeled according to their diffraction order. The dashed line at zero degrees defines the direction of the direct beam from the synchrotron. The model used $k = 2000, \alpha = 2.8^o$, $\varepsilon = 0.17^o$, $p = 574$ nm, $b/p = 0.176$, and $a = 473$ nm, corresponding to the narrowest part of the grating slits.

inclined by 0.17^o from the normal by a model consisting of a pyramid of twenty 500 nm-tall rectangles with widths ranging from 99.5 nm for the layer at the bottom to 40.2 nm for the topmost layer. The index of refraction of silicon is taken from Ref. [25]. The angle of incidence α for the simulation is chosen to be 2.8^o in accordance with experimental conditions.

Experimental results and theoretical predictions with no adjustable parameters follow each other qualitatively over the entire range of measurements. Noticeable is the high diffraction efficiency, with individual orders showing up to 46% efficiency. The sum of blazed order efficiencies at most wavelengths ranges from 28-55% and 29-70% for data and theory, respectively. Starting at the longest wavelength, diffraction in -1st order is close to the blaze condition and dominates the transmitted intensity. As the wavelength becomes shorter the -1st order peak moves away from the blaze condition towards smaller angles, while the -2nd order peak moves into the blaze region from larger angles. This behavior repeats for higher orders towards shorter wavelengths until eventually θ_c, which is proportional to λ, becomes smaller than the angle of incidence onto the grating sidewalls. At shorter wavelengths the mirrors will become increasingly transparent and 0th order transmission increases while the blazing effect gradually diminishes. We were able to observe blazing for up to -33rd order at $\lambda = 1.62$ nm, but individual peaks were difficult to resolve due to limited dispersion. For most of the data from Fig. 5 the measured diffraction efficiency, summed over the peaks close to the blaze condition, amounts to 70-85% of the theoretical prediction. All the shown data was obtained on a single spot on the grating. However, measured diffraction efficiencies vary as a function of beam position on the grating sample, which we believe to be due to inhomogeneities in processing that lead to structural defects [23].

#94888 - $15.00 USD Received 14 Apr 2008; revised 15 May 2008; accepted 22 May 2008; published 28 May 2008

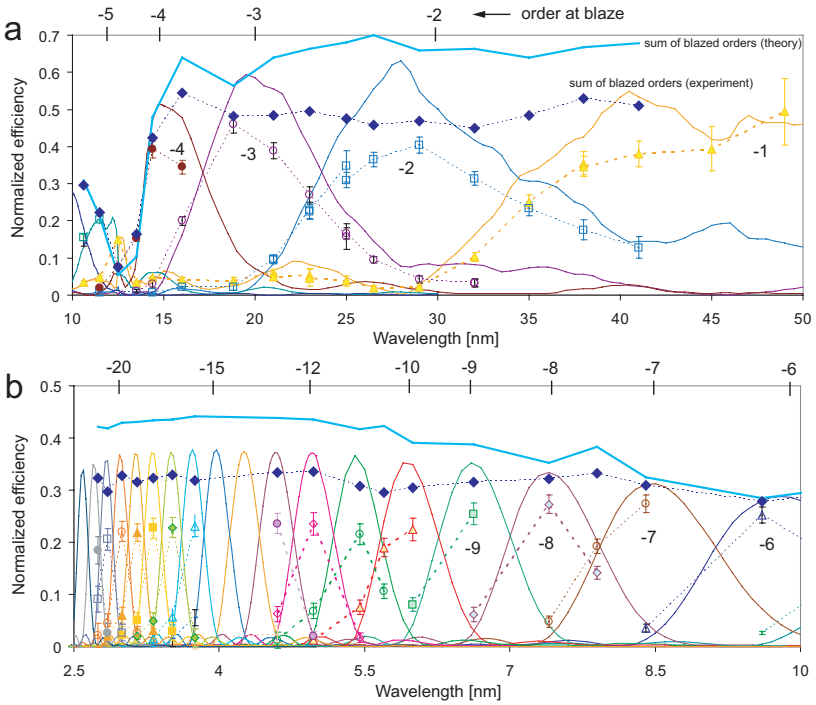

Fig. 6. Normalized diffraction efficiency. (a) 10 - 50 nm wavelengths. (b) 2.5 - 10 nm wavelengths. Data are shown with error bars. We fit diffraction peaks to Gaussians and obtain error bars from estimates of standard errors. Data points corresponding to a fixed diffraction order are connected by dashed or dotted lines to guide the eye. Theoretical RCWA results for each order are drawn with solid lines. The sum of diffracted intensities close to the blaze condition is shown at the measured wavelengths with black diamonds. The solid line above shows the predicted sum of the same orders at the same wavelengths. The wavelengths that fulfill the blazing condition are labeled according to diffraction order m above each graph. The dip in diffraction efficiency around $\lambda = 13$ nm is due to the silicon L absorption edges.

4. Discussion

We have introduced and demonstrated a nearly absorption-free transmission grating design based on sub critical-angle reflection off of nanometer-scale mirrors that enables blazing and highly efficient broadband diffraction for EUV and soft x-ray photons. The experimentally observed diffraction efficiencies are close to theoretical predictions. We believe that structural imperfections that limit diffraction efficiency can be reduced further by improvements in the fabrication process. Similarly, changes in support mesh design and fabrication steps are expected to lead to imperative increases in the open area fraction.

We are currently developing CAT gratings with a period of 200 nm. Our goal is to reach a period of 100 nm, where Si CAT gratings are expected to produce $>$ 50% efficiency at blaze throughout the $\lambda =$ 1-4 nm band, and an open area fraction ≥ 0.9 [20]. Furthermore, grating bars that are inclined by some angle relative to the grating normal can be fabricated from SOI wafers that are intentionally miscut from the $<$110$>$ plane.

Efficient blazing enables the use of higher diffraction orders [26], which increases spectral resolution in spectrometer applications up to *m*-fold [20]. CAT gratings therefore combine the

#94888 - $15.00 USD Received 14 Apr 2008; revised 15 May 2008; accepted 22 May 2008; published 28 May 2008

advantages of transmission gratings and blazed reflection gratings with low polarization sensitivity. (RCWA calculations predict $\ll 1\%$ relative diffraction efficiency difference between TE and TM polarization states for typical CAT grating configurations.)

CAT gratings could be useful in many applications such as x-ray spectroscopy telescopes for astronomy [20, 27], or highly efficient transmission gratings in x-ray phase imaging applications and grating interferometers [28, 29, 30]. The CAT grating design can also readily be applied to the fabrication of soft x-ray focusing devices such as linear zone plates [31] and allows the use of higher order foci - and thus higher resolution - with high efficiency [26, 32]. Its high broadband efficiency enables the applicability of a single CAT grating over a range of wavelengths. Such a grating might be able to replace numerous narrow-band multilayer based elements (e.g. beam splitters [33]) that otherwise have to be fabricated separately for each wavelength of interest. Use as an efficient analyzer grating for soft x rays or EUV photons could reduce dose exposure for biological specimen. In general, the existence of high-efficiency blazed broadband transmission gratings opens a whole new design space for soft x-ray and EUV optics and instruments.

Our fabrication approach relies on the high etch anisotropy of Si crystals in aqueous alkaline solutions and thus links the reflectivity of the grating bar sidewalls to the index of refraction for Si. However, the reflectivity could be modified similar to the case of grazing-incidence x-ray mirrors through coating of the grating bars with a few nm of a different material, e.g., via atomic layer deposition [34]. Simulations indicate that broadband diffraction efficiencies $> 40\%$ could be achieved at x-ray energies up to several keV.

Apart from photons, CAT gratings for cold neutrons ($\lambda_{deBroglie} \sim 1$ nm) could be fabricated on a solid substrate, and scattering length density contrast - and therefore θ_c - could be increased through thin coatings of Ni on Si.

Most objects will reflect efficiently from a smooth enough surface at low enough grazing angles of incidence [35, 36]. As a rule of thumb a critical angle can be estimated by $2\pi\sigma\sin\theta_c = \lambda_{deBroglie}$, where σ is the roughness of the surface. While CAT gratings might also be suitable for the blazed diffraction of atoms [2], electrons [37, 38], molecules [3], and clusters [39], reflection of such particles in the long grating channels probes more complicated surface potentials and internal particle excitations that cannot be described by a simple discrete change in the index of refraction. However, the many μm-long interaction distance in the narrow grating slits could enhance the sensitivity of diffraction patterns to particle-surface interactions [40] and internal states [41], whether in a blazed configuration or at normal incidence.

Acknowledgments

We acknowledge technical support from R. Fleming, J. Daley, C.-H. Chang, and Y. Zhao (MIT) and A. Aquila and F. Dollar (ALS). We thank K. A. Flanagan, A. D. Cronin, and T. O'Reilly for helpful conversations. We acknowledge facilities support from the Space Nanotechnology Laboratory, the Nanostructures Laboratory, and the Microsystems Technology Laboratory (MIT). This work was supported in part by grant NNX07AG98G from the National Aeronautics and Space Administration. M.A. was supported by a Samsung Fellowship. The Advanced Light Source at Lawrence Berkeley National Laboratory is supported by the Director, Office of Science, Office of Basic Energy Sciences, Materials Sciences Division, of the U.S. Department of Energy under Contract No. DE-AC02-05CH11231.

#94888 - $15.00 USD Received 14 Apr 2008; revised 15 May 2008; accepted 22 May 2008; published 28 May 2008